applied optics

Design of optical anapole modes of all-dielectric nanoantennas for SERS applications

Debao Wang,[1] Jingwei Lv,[1,*] Jianxin Wang,[1] Yanru Ren,[1] Ying Yu,[1] Wei Li,[1] Paul K. Chu,[2] and Chao Liu[1]

[1]School of Physics and Electronic Engineering, Northeast Petroleum University, Daqing 163318, China
[2]Department of Physics, Department of Materials Science and Engineering, and Department of Biomedical Engineering, City University of Hong Kong, Tat Chee Avenue, Kowloon, Hong Kong, China
*lvjingwei2009123@126.com

Received 26 April 2023; revised 17 June 2023; accepted 19 June 2023; posted 21 June 2023; published 7 July 2023

To obtain large electric field enhancement while mitigating material losses, an all-dielectric nanoantenna composed of a heptamer and nanocubes is designed and analyzed. A numerical simulation by the finite element method reveals that the nanoantenna achieves the optical electric anapole modes, thereby significantly enhancing the coupling between different dielectrics to further improve the near-field enhancement and spontaneous radiation. Field enhancement factors $|E/E_0|^2$ of 3,563 and 5,395 (AM1 and AM2) and a Purcell factor of 3,872 are observed in the wavelength range between 350 and 800 nm. This nanoantenna has promising potential in applications involving surface-enhanced Raman scattering and nonlinearities due to its low cost and excellent compatibility.

https://doi.org/10.1364/AO.494145

1. INTRODUCTION

Nanostructures composed of metallic and dielectric components can enhance light—matter interactions, while simultaneously confining light in the subwavelength range. These structures deliver superior performance due to the near-field enhancement and large mode volume [1–3]. By precisely promoting the coupling of different resonance modes in hybrid metal-dielectric nanostructures, fascinating optical phenomena such as the nonradiative state [4–6] and Fano resonance [7,8] have been investigated, and recent pertinent advances have spurred the rapid development of applications in nonlinearities [9–11], surface-enhanced Raman scattering (SERS) [12], quantum imaging [13,14], and sensing [15–17].

Metal nanostructures or hybrid nanostructures consisting of metallic and dielectric components have been studied recently to accomplish near-field enhancement [18,19]. Yao *et al*. have increased the field strength by combining metallic and dielectric components in the anapole mode to exploit the mirror effect [20]. Although advances have been made in the near field, material losses arising from the metal imaginary part are still unavoidable. Therefore, the use of materials with large refractive indices to eliminate intrinsic absorption, external heating, and material loss while retaining greater freedom has become a new strategy to enhance the electric field intensity and biosensing [21,22]. For example, Soret colloids [23], nanostructured carbon flowers [24], high refractive index Nd_2O_3 nanorods [25], and TiCN nanocubes [26] have been studied in the surface plasmon coupled emission (technique. In addition, various methods have been proposed to prepare all-dielectric nanostructures. For instance, Liu *et al*. have achieved the perfect anapole mode effect and enhanced the electric field by stacking two simple silicon (Si) nanodisks [27]. The anapole mode is a radiation-free resonance derived from the destructive interference between the electric dipole (ED) and toroidal dipole (TD) moments [28]. In particular, TD is not a third source of the electromagnetic field independent of the electric and magnetic dipoles (MDs), but is strictly a higher order term of the ED. Nonetheless, conventional anapole modes have drawbacks such as the limitation of the single material and lack of apparent near-field enhancement. Prior studies have predominantly observed one single anapole mode, but the physical mechanism of the significant near-field enhancement by excitation of the dual anapole mode is still not well understood.

Herein, a nanoantenna composed of two high refractive index dielectric materials is designed. The structure composes a Si substrate, a thin silica film as the spacer, and a heptamer of Si. The coupling between the dielectrics is enhanced, resulting in a substantially enhanced electric field and realization of the double electric anapole mode. The coupling process between the dielectrics is discussed, and the optimal structural parameters are determined. An analysis of the Purcell factor (PF) reveals that the structure has positive effects in the modulation of spontaneous radiation by the nano-resonators. The nanoantenna which provides near-field enhancement and self-luminous properties is suitable for applications in the realms of SERS and nonlinearities.

2. MULTIPOLE COMPOSITION METHOD

The multipole decomposition method is employed to unambiguously analyze the scattering properties by representing the total scattering cross section (SCS) as a sum of contributions of different dipole moments [29,30,31]. In the spherical coordinate system, the multipole expansion usually includes the ED moment P_α, MD moment M_α, TD moment T_α, electric quadrupole moment $Q^e_{\alpha\beta}$ (EQ), and magnetic quadrupole moment $Q^m_{\alpha\beta}$ (MQ), and the definitions are shown below [32]:

$$\boldsymbol{P}_\alpha = \frac{1}{i\omega}\int \boldsymbol{J}_\alpha \mathrm{d}^3\boldsymbol{r}, \tag{1}$$

$$\boldsymbol{M}_\alpha = \frac{1}{2c}\int [\boldsymbol{r}\times\boldsymbol{J}]_\alpha \mathrm{d}^3\boldsymbol{r}, \tag{2}$$

$$\boldsymbol{T}_\alpha = \frac{1}{10c}\int \left[(\boldsymbol{r}\cdot\boldsymbol{J})_{r_\alpha} - 2r^2\boldsymbol{J}_\alpha\right]\mathrm{d}^3\boldsymbol{r}, \tag{3}$$

$$\boldsymbol{Q}^e_{\alpha\beta} = -\frac{1}{i\omega}\int \left[r_\alpha \boldsymbol{J}_\beta + \boldsymbol{J}_\alpha r_\beta - \frac{2}{3}\delta_{\alpha\beta}(\boldsymbol{r}\cdot\boldsymbol{J})\right]\mathrm{d}^3\boldsymbol{r}, \tag{4}$$

$$\boldsymbol{Q}^m_{\alpha\beta} = \frac{1}{3c}\int \left[[\boldsymbol{r}\times\boldsymbol{J}]_\alpha r_\beta + r_\alpha[\boldsymbol{r}\times\boldsymbol{J}]_\beta\right]\mathrm{d}^3\boldsymbol{r}, \tag{5}$$

where $\boldsymbol{r}$ is the positive vector, and the subscripts $\alpha, \beta = x, y, z$ denote the components of EQ and MQ.

The anapole mode produced by the all-dielectric nanoantenna depicted in Fig. 1 is composed of two simple cubes made of Si and silica, and the heptamer is composed of Si. The plane wave is linearly polarized along the x axis, and propagation is parallel to the y axis (red symbol). The diameter and height of the cylinders forming the Si heptamer are D = 100 nm and h = 50 nm, and the gap between the cylinders is G = 0.5 nm. In addition, a Si cube with a height H_1 of 50 nm and length L_1 of 300 nm is chosen as the substrate considering the manufacturability of the structure. Meanwhile, a SiO_2 layer with a length L_2 of 300 nm and height H_2 of 5 nm is introduced between the heptamer and substrate as the gain medium to boost the near-field interactions and enhance the coupling between the heptamer and substrate [19]. The refractive index of the Si medium is 3.5, and the dielectric constant of SiO_2 is obtained from Palik's book [33]. The all-dielectric nanostructure is placed in the air with a refractive index of $n = 1.0$, and the electromagnetic field is analyzed by the finite element method based on COMSOL 6.0 Multiphysics.

3. RESULTS AND DISCUSSION

In order to elucidate the physical mechanism, the optical characteristics of the dielectric substrates (the combination of SiO_2 and Si nanocubes) are studied. Figures 2(a) and 2(b) exhibit the SCS and electric field intensity $|E/E_0|^2$ of the dielectric substrates (shown in the inset) from 319 to 800 nm. Two distinct dips are observed in the scattering spectrum at the wavelength of $\lambda = 397$ nm and $\lambda = 604$ nm. Correspondingly, in the electric field enhancement curve, the maximum values are observed with the $|E/E_0|^2$ up to 2.8 and 5.7. Furthermore, the contribution of different multipoles to the total SCS of the combination of SiO_2 and Si nanocubes (shown in the inset) is also calculated, as shown in Fig. 2(c). It can be seen that the contribution of the other multipoles is negligibly small at the resonance wavelengths of $\lambda = 397$ nm and $\lambda = 604$ nm. The sharp reduction of the SCS at these two wavelengths mainly originates from the destructive interference between the ED and TD moments, which is known as the electric anapole mode [28].

In order to better demonstrate the coupling between different structures and dielectric substrates (the combination of Si and SiO_2 cubes), the trimer, pentamer, heptamer, and octamer of Si are introduced to the surface of the dielectric substrates, and the calculated SCS and electric field enhancement factor $|E/E_0|^2$ are given in Fig. 3. It can be observed in Figs. 3(a)–3(d) that the introduction of these four structures significantly enhances the electric field enhancement compared to the individual dielectric substrates, which is attributed to the strong coupling effect between the dielectric substrates and the introduced structures. Figures 3(a) and 3(b) exhibit the scattering and electric field enhancement properties of the trimer and pentamer, respectively. The locations of the two distinct dips of the SCS correspond to the two peaks of the electric field enhancement, which is consistent with the theory of the anapole mode of field enhancement stemming from the spatial overlap and destructive interference between multipoles [34]. However, the difference is that the obtained $|E/E_0|^2$ is obviously distinct. For the

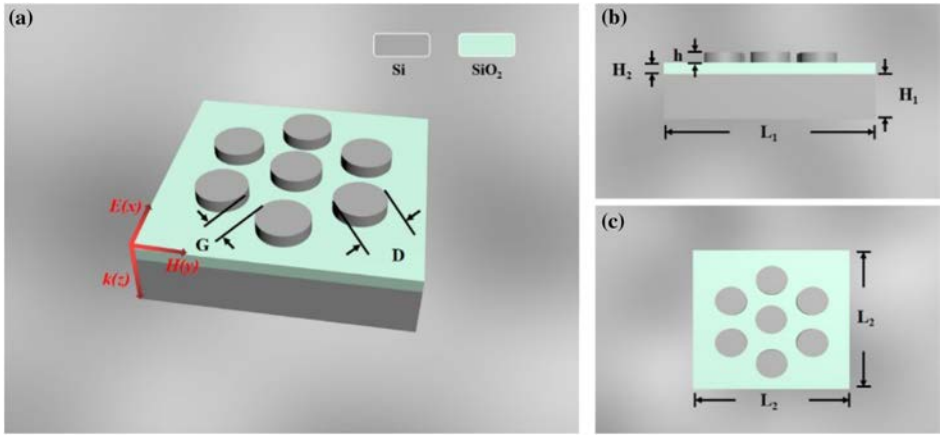

Fig. 1. (a) Schematic diagram of the three-dimensional nanoantenna. (b) Front view and (c) top view of the nanoantenna.

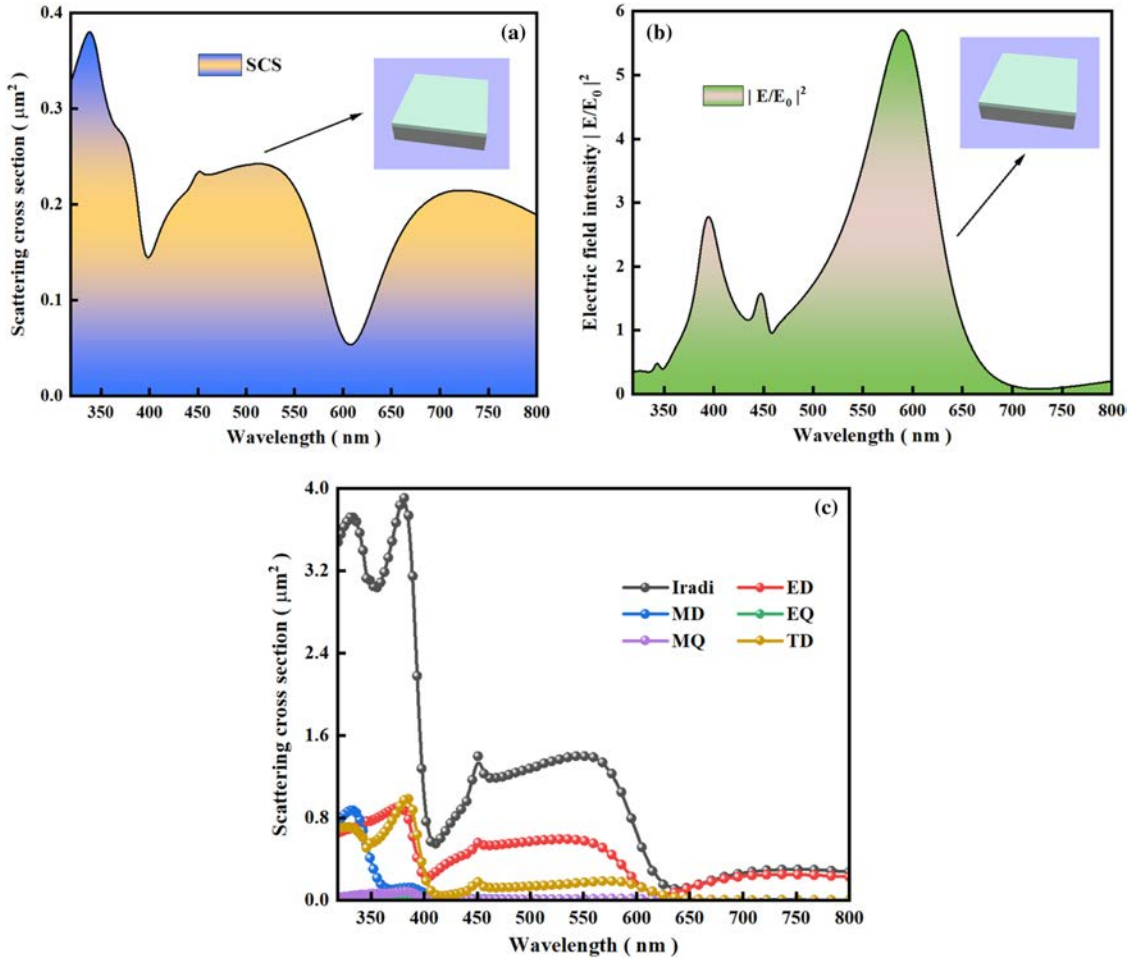

Fig. 2. Schematic diagram of the (a) SCS, (b) electric field enhancement factor $|E/E_0|^2$, and (c) multipole decomposition of the dielectric substrates. The illustrations in (a) and (b) depict the structure of the dielectric substrates.

trimer, the near-field enhancement $|E/E_0|^2$ of 500 and 4282 are acquired at the wavelength of $\lambda = 401$ nm and $\lambda = 637$ nm. For the pentamer, the near-field enhancement $|E/E_0|^2$ of 1324 and 3338 are obtained at wavelengths of $\lambda = 420$ nm and $\lambda = 653$ nm. Furthermore, the SCS spectrum and near-field enhancement of the Si heptamer nanostructure are investigated as shown in Fig. 3(c). Four prominent resonance peaks and three dips emerge from the scattering spectra. Compared with the trimer and pentamer, this nanoantenna has a larger SCS of up to 0.42 μm^2, which greatly improves the scattering efficiency. In addition, it is seen that the field enhancement curves of this structure disclosing field enhancement factors is about 3563 and 5395 at wavelengths of 420 and 661 nm, respectively, which is obviously greater than the trimer and pentamer. As depicted in Fig. 3(d), the anapole mode is implemented at the wavelength of 449 nm, and the electric field enhancement is about 27. Therefore, compared with the other three structures, the nanostructure composed of the Si heptamer, together with the SiO_2 and Si nanocubes, has better optical properties; thus, it is selected to be used for the follow-up study.

To study the underlying mechanism of the anapole mode, we conduct multipole decomposition of the proposed nanoantenna in the wavelength range between 350 and 800 nm, as shown in Fig. 4. The two enlarged illustrations depicted in the left and right insets provide clear evidence of a significant tilt in the ED moment [35]. The two dips at incident wavelengths of $\lambda = 420$ and 661 nm are the excitation of the first-order and second-order anapole modes, namely AM1 and AM2, respectively. By comparing the dielectric substrates (the combination of Si and SiO_2 cubes) shown in Fig. 2(c), it is found that the trend of multipole decomposition of the proposed all-dielectric nanoantenna is extremely similar to that of the dielectric substrates. They are both optical anapole modes further realized by the destructive interference between the ED moment and TD moment. The difference is that there is a significant enhancement of the electric field intensity at AM1 and AM2, which indicates that the introduced Si heptamer plays a crucial role in the improvement of the electric field intensity. In other words, the all-dielectric nanoantenna retains the radiation-free properties of the dielectric substrates at AM1 and AM2, while taking advantage of the Si heptamer to promote the coupling between the Si heptamer and the dielectric substrates. The results indicate that the electric field enhancement is remarkably improved by the coupling of the dielectric substrates and the Si heptamer.

According to our analysis of the field enhancement, the electric and magnetic field distributions of the all-dielectric

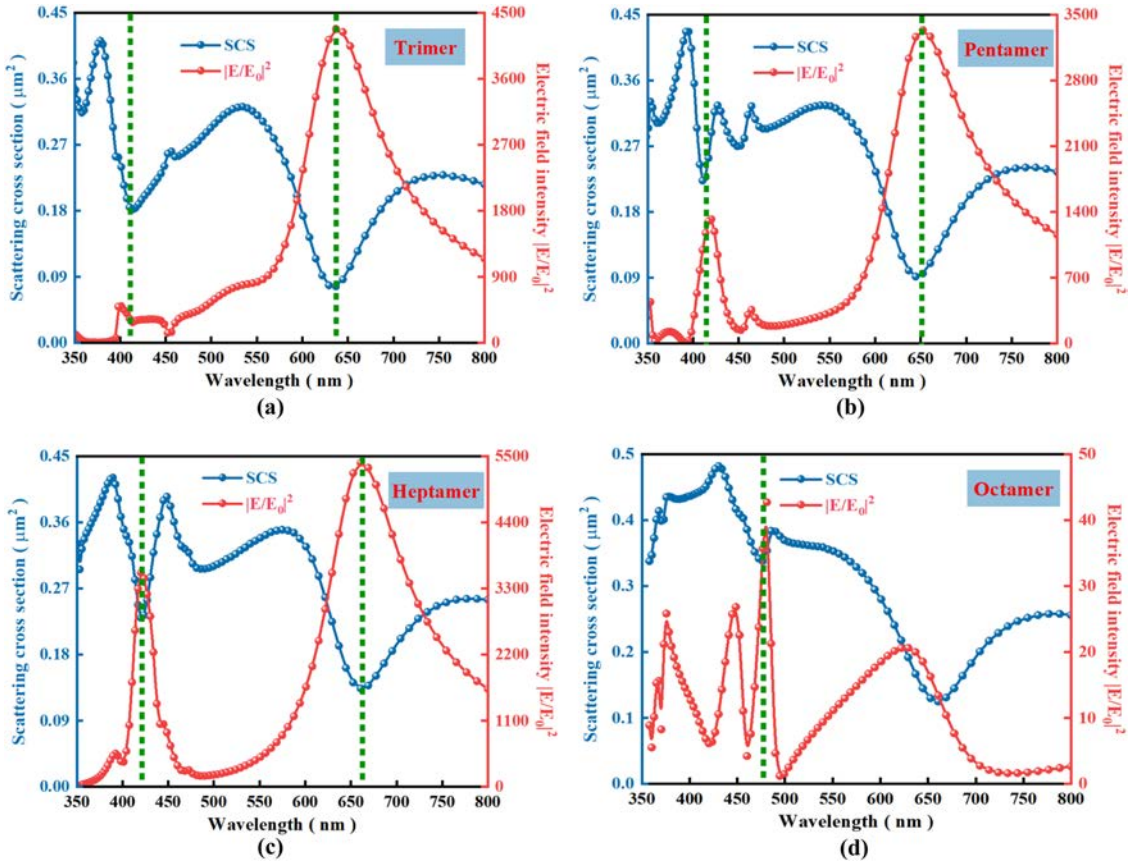

Fig. 3. Schematic diagram of the SCS and electric field enhancement factor $|E/E_0|^2$ for the (a) trimer, (b) pentamer, (c) heptamer, and (d) octamer. The green dashed line indicates the resonant wavelength at which the anapole mode is located.

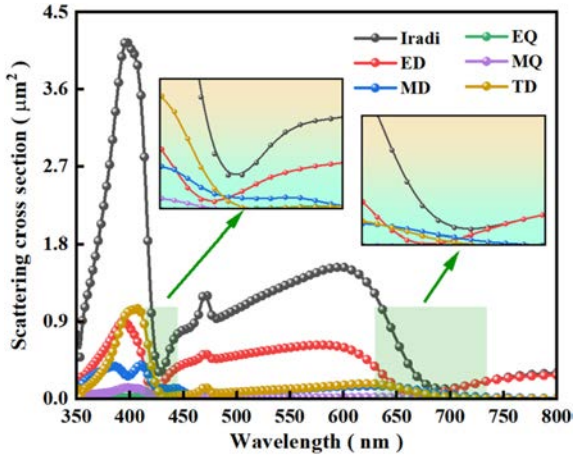

Fig. 4. Multipole decomposition of the all-dielectric nanoantenna with the insets showing the two enlarged regions.

nanoantenna for the AM1 and AM2 modes corresponding to wavelengths of 420 and 661 nm, respectively, are presented in Fig. 5. Figure 5(a) shows that the high electric field is concentrated at the edges and junctions of the cylinders, which is due to the fact that the electrons of the cylinders composed of the heptamer are excited to move to the edges. The magnetic field distribution in Fig. 5(b) illustrates that all the columns have a relatively large magnetic field strength, particularly on the junctions. The electric and magnetic field distributions of the AM2 mode at 661 nm are plotted in Figs. 5(c) and 5(d). The electric and magnetic field features are stronger in comparison with the AM1 mode. The field is almost entirely distributed in the gap between the middle column and surrounding six columns in Fig. 5(c), thus generating two distinct hot spots in the magnetic field shown in Fig. 5(d).

Many types of all-dielectric nanoantennas have been proposed recently to exploit the effects of the electric field enhancement factor $|E/E_0|^2$. Nevertheless, the structural limitations hamper the apparent field enhancement, and there is still room for improvement. As listed in Table 1, a single-layer SiO_2 nanodisk and Si nanoring or even double-layer AlGaAs nanodisks are not effective for electric field enhancement. In contrast, if a Si nanodisk is simply modified (e.g., by removing the hole at the center), the electric field enhancement performance will be significantly improved up to a value of 100. Further, the configuration of complex dielectric structures also plays a crucial role in the improvement of the near-field electric field. For example, the combination of the perforated Si nanodisk and WSe_2 achieve an electric field enhancement effect of nearly 100. The structure described in this paper exhibits a notable electric enhancement performance, which can be attributed to two factors. On the one hand, the complexity of structures strongly promotes light—matter interactions. On the other hand, the Si

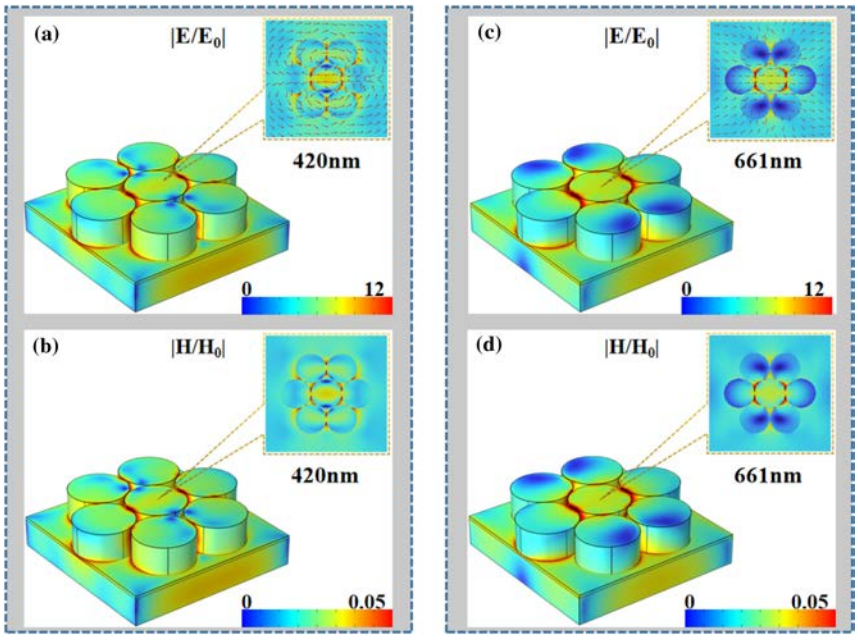

Fig. 5. (a), (b) Electric and (c), (d) magnetic field distributions of the nanoantenna at wavelengths of 420 and 661 nm with the insets showing the xoy plane.

Table 1. Comparison of the Properties of All-Dielectric Nanoantenna with the Electric Field Enhancement Factor $|E/E_0|^2$

References	Characteristics	Wavelength range (nm)	$\lvert E/E_0\rvert^2$	Structure diagram
[36]	21 nm—thickness SiO_2 layer	200–1000	35	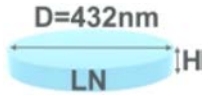
[37]	Si nanodisk with rectangular holes	600–800	100	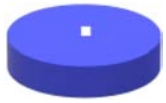
	Combination of perforated Si nanodisk and WSe_2	600–800	100	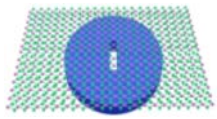
[38]	Double-layer AlGaAs nanodisks with gaps	350–800	80	
	Combination of double-layer AlGaAs nanodisks and GaAs cylinder	350–800	60	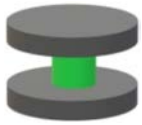
[16]	Si nanoring	500–1000	8	
This work	Combination of Si and SiO_2 nanostructure	350–800	5395	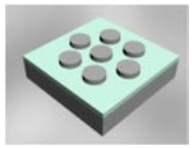

heptamer structure facilitates the coupling of electric hot spots to the surface of the substrate.

The structural parameters play a significant role in the scattering efficiency improvement and field enhancement. Figures 6(a)–6(i) show the process of optimization of the three different parameters, including the diameter D, height h of the cylinders, as well as the gap between the cylinders. As depicted in Figs. 6(a)–6(c), three resonance peaks of the SCS and thus two dips emerge from the SCS spectrum. The SCS broadens at multiple wavelengths and exhibits a redshifting trend when the diameter D is increased from 50 to 100 nm. It is of interest that three resonance peaks continuously widen as the diameter increases, which can be attributed to the fact that the increase of contact area can intensify the coupling between the cylinders, while the electric field of the AM1 and AM2 modes increases apparently. In essence, the extent of the electric field improvement varies because of the difference in the ED and TD interactions, as exemplified by the AM1 mode and AM2 mode. The interaction between ED and TD at AM1 mode is significantly weaker than that at AM2, thus leading to a much higher electric field intensity at AM2 than at AM1. According to Figs. 6(d)–6(f), when the gap G is varied from 0.5 to 5 nm, it presents a slight blueshifting trend on the SCS, which indicates that the improvement in the scattering efficiency is not sensitive to the variation of the intervals while the electric field enhancement factors of AM1 and AM2 decrease sharply. This result demonstrates that there is a strong correlation in the field enhancement. It can be interpreted that increasing the gap decreases the degree of intercolumnar coupling and weakens the interactions between electrons. Further calculation and analysis of the effects of the structural parameter (height of the heptamer) on the SCS and field enhancement are presented

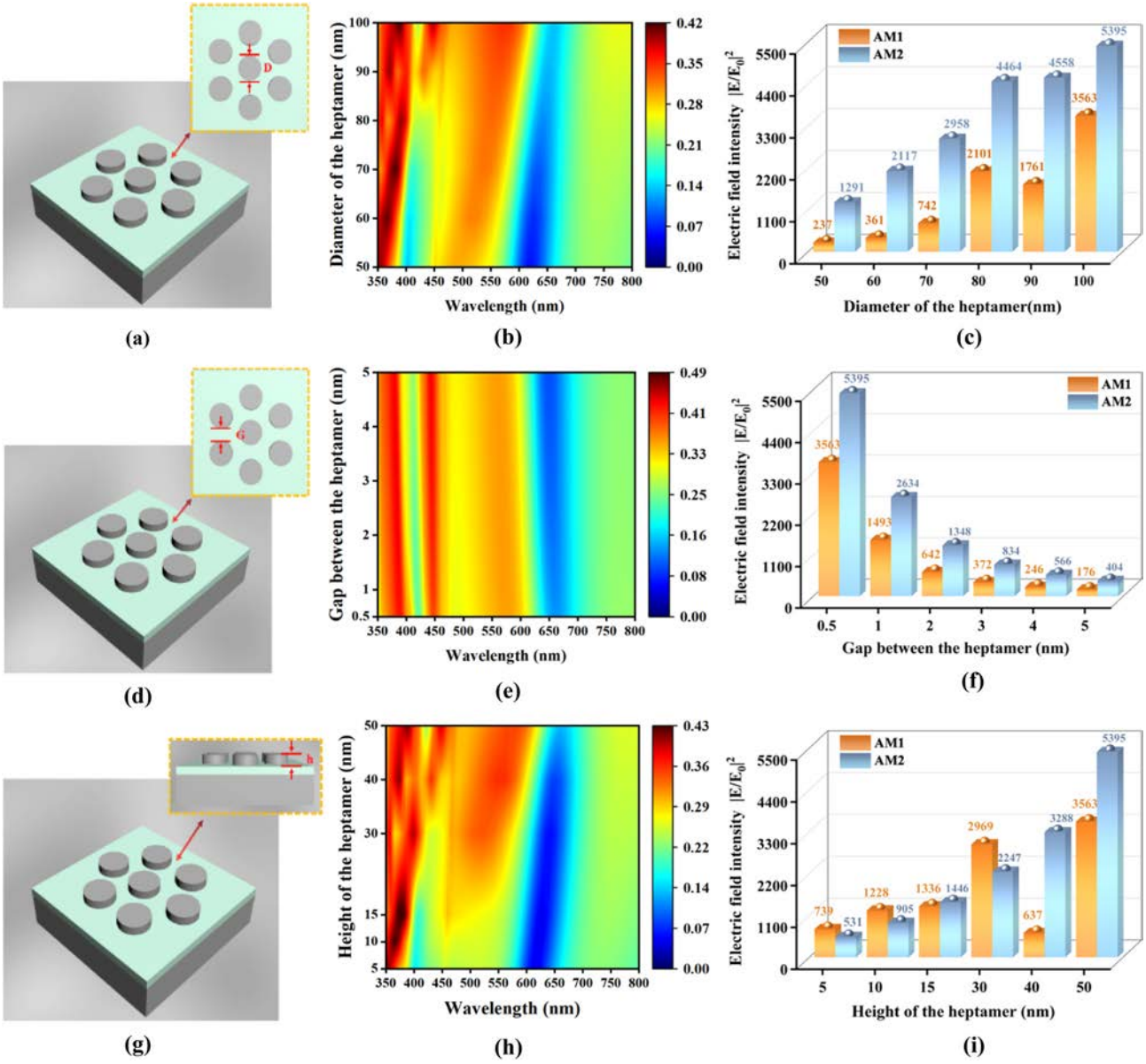

Fig. 6. (a), (d), (g) Schematic diagram of the nanostructure for different structural parameters of D, G, and h. (b), (e), (h) Dependence of the SCS on wavelengths for D, G, and h. (c), (f), (i) Influence of parameters D, G, and h on the electric field of the AM1and AM2 modes.

in Figs. 6(g)–6(i). Figure 6(h) shows the dependence of the SCS on the resonance wavelength for different heights of the cylinders (5–50 nm). As the height h increases, three resonance wavelengths shift to a longer wavelength, and the interaction between the cylinders increases, thus significantly improving the scattering efficiency. Therefore, as the height increases, a greater number of electrons migrate to the edge of the cylinders and are excited by photons in the nanostructure. Figure 6(i) describes the relationship between the height and electric field enhancement $|E/E_0|^2$ of the AM1 and AM2 modes. The field enhancement increases initially and then decreases as h is varied from 5–50 nm, while AM2 presents a continuous increasing trend. The results demonstrate that different structural parameters produce different degrees of coupling. In contrast to the field feature of AM1, the electric field of AM2 displays an upward trend with heights, and it is significantly higher than that of AM1 for a height of 50 nm. The optimal height parameter is determined to be h = 50 nm by considering the SCS in Fig. 6(h). Based on our analysis, it is evident that optimization of the structural parameters yields higher scattering efficiency and electric field enhancement.

Enhancing the near-field capabilities of nanoantennas not only is beneficial to electronics, but also has a large potential in optimizing spontaneous radiation [39]. In general, the properties of the ED emission in nanostructures can be measured by the PF, as shown by the following equation [40]:

$$\mathrm{PF} = \frac{P}{P_0}, \tag{6}$$

$$P_0 = \frac{\omega^4 |P_0|^2}{12\pi\varepsilon_0 c^3}, \tag{7}$$

where $\boldsymbol{P_0}$ and $\boldsymbol{P}$ are the vacuum power loss without a resonator and the emission power of an ED emitter with a resonator, separately.

To evaluate the performance of our structure as a quantum emitter, an ED source is placed in the gap of the cylinders of the heptamer at positions A (0, 87, 25), B (25, 43.5, 25), C (87, −50.25, 25), and D (50.25, 0, 25), as shown by the inset in Fig. 7(a), which shows the relationship between the PF values at these four points and the resonance wavelength. The PF value of the ED source at λ = 437 nm is approximately 3872. In comparison with other all-dielectric structures, our structure is more effective in enhancing spontaneous radiation.

In addition, it is important to note that the dipole moment in scattering multipoles is defined in terms of the source located at the center of radiation. In this case, the radiation center of the nanostructure is perfectly in agreement with the geometric center. However, in instances where the displacement of this center occurs as a result of experimental or fabrication discrepancies, it is clear that the scattering multipoles calculated using this method are inaccurate [41]. To evaluate the impact of this error on the scattering multipoles, intensities of the radiated dipoles of the shifted electric source over its shift for these two nanostructures (dielectric substrate and the all-dielectric nanostructure) at AM1 and AM2 are given, as shown in Figs. 7(b)–7(e). Among them, the point (0, 0, 0) is defined as the center of the radiation. It is located on the −z axis when the value is less than 0. According to Figs. 7(b) and 7(c), it can be inferred that the scattering multipoles show a decreasing trend, and the curves are axisymmetric curves when the shifted source moves toward the +z axis or the −z axis, which indicates that the radiation center has a clear symmetry for the dielectric substrate structures. Furthermore, the intensities of the radiated

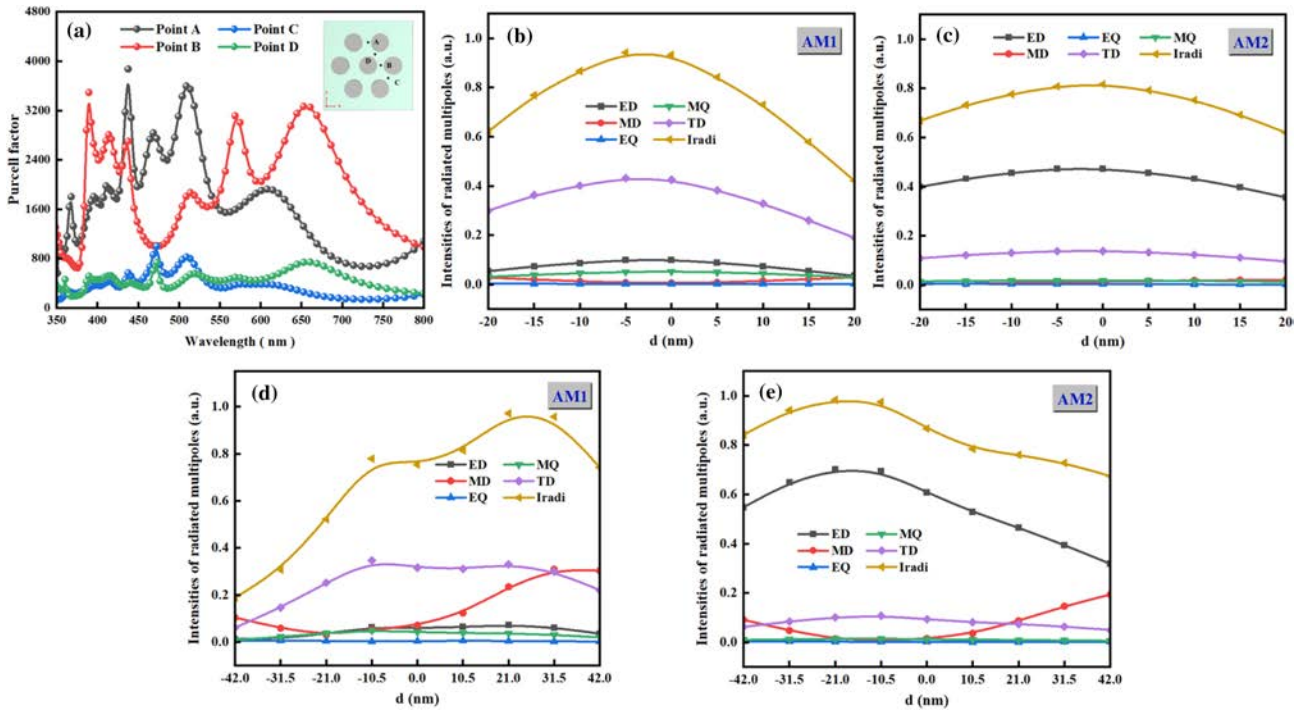

Fig. 7. (a) PFs of the ED emitter at the four points with the inset showing the locations. (b) and (c) Intensities of the radiated dipoles of the shifted electric source over its shift for the dielectric substrate at AM1 and AM2 modes. (d) and (e) Intensities of the radiated dipoles of the shifted electric source over its shift for the all-dielectric nanostructure at AM1 and AM2 modes.

Table 2. Comparison between Our Nanoantenna and Recently Reported All-Dielectric Nanoantennas

References	Characteristics	Wavelength range (nm)	Purcell factor
[42]	The gold dimer	400–800	∼300
	The Si dimer		∼80
[43]	All-dielectric Si nanoparticle (SiNP)	20–200	∼25
[44]	Si cuboid dielectric	400–850	∼18
[45]	Ring in free space	600–750	∼900
This work	Combination of Si and SiO_2 nanostructure	350–800	3872

dipoles of the shifted electric source over its shift for the all-dielectric nanostructure are also depicted in Figs. 7(d) and 7(e). In contrast to the dielectric substrate, it is clear that the radiation center is asymmetric according to the curve.

In recent years, different kinds of all-dielectric nanoantennas have been designed, especially enhanced quantum emitters (characterized by the PF). Nevertheless, it is widely acknowledged that achieving reinforced spontaneous radiation from an all-dielectric nanoantenna is a challenging task due to the strong correlation between the electric field and spontaneous radiation. In this respect, our structure has excellent radiation characteristics as an ED emitter as shown in Table 2.

Although there has been considerable advancement in the exploration of different nanomaterials at subwavelength scales, a number of limitations remain. (1) Conventional anapole modes have drawbacks such as the limitation of the single material and lack of apparent near-field enhancement. (2) Prior studies have predominantly observed one single anapole mode, but the physical mechanism of the significant near-field enhancement by excitation of the dual anapole mode is still not well understood. This report helps to address two challenges currently encountered by proposing the all-dielectric nanoantenna consisting of the combination of the Si heptamer and the dielectric substrates. This nanoantenna demonstrates that the excitation of the anapole mode and the improvement of the near-field electric field performance can be significantly induced by promoting the coupling interaction between different single dielectric structures. This simulation work opens a window for flexible manipulation of the optical properties of nanoantennas that can be applied in SERS [23] and transdisciplinary nanophotonics [25,46] applications.

4. CONCLUSION

What we believe to be a novel all-dielectric nanoantenna composed of Si and silica is designed and analyzed. This nanoantenna realizes optical electric anapole modes at multiple wavelengths, consequently overcoming the limitation of conventional all-dielectric nanostructures which can only realize a single anapole mode and shows insignificant electric field improvement. Our theoretical assessment reveals that the nanoantenna delivers great modulation performance for spontaneous radiation such as field enhancement factors $|E/E_0|^2$ of 3,563 and 5,395 (AM1 and AM2), as well as a PF of 3,872 for the optimized structure. The significant results and application potential are expected to guide future research in the fields of nonlinearities and quantum emissions.

Funding. Outstanding young and middle-aged research and innovation team of Northeast Petroleum University (KYCXTD201801); Natural Science Foundation of Heilongjiang Province (LH2021F007); China Postdoctoral Science Foundation (2020M670881); Study Abroad Returnees Merit-based Aid Foundation in Heilongjiang Province (070-719900103); Northeastern University scientific research projects (2019KQ74); Strategic Research Fund of the City University of Hong Kong (SRG) (7005505).

Disclosures. The authors declare no conflicts of interest.

Data availability. Data underlying the results presented in this paper are not publicly available at this time but may be obtained from the authors upon reasonable request.

REFERENCES

1. D. Tzarouchis and A. Sihvola, "Light scattering by a dielectric sphere: perspectives on the Mie resonances," Appl. Sci. **8**, 184 (2018).
2. S. Raza and A. Kristensen, "Raman scattering in high-refractive-index nanostructures," Nanophotonics **10**, 1197–1209 (2021).
3. H. Ahmed and V. E. Babicheva, "Resonant and scattering properties of tungsten disulfide WS_2 nanoantennas," in *Conference on Photonic and Phononic Properties of Engineered Nanostructures* (2020).
4. X. Li, J. Yin, J. Liu, F. Shu, T. Lang, X. Jing, and Z. Hong, "Resonant transparency of a planar anapole metamaterial at terahertz frequencies," Photonics Res. **9**, 125–130 (2021).
5. G. Labate, A. K. Ospanova, N. A. Nemkov, A. A. Basharin, and L. Matekovits, "Nonradiating anapole condition derived from Devaney-Wolf theorem and excited in a broken-symmetry dielectric particle," Opt. Express **28**, 10294–10307 (2020).
6. A. A. Basharin, E. Zanganeh, A. K. Ospanova, P. Kapitanova, and B. A. Evlyukhin, "Selective superinvisibility effect via compound anapole," Phys. Rev. B **107**, 155104 (2023).
7. L. Yang, S. Yu, H. Li, and T. Zhao, "Multiple Fano resonances excitation on all-dielectric nanohole arrays metasurfaces," Opt. Express **29**, 14905–14916 (2021).
8. A. E. Miroshnichenko and Y. S. Kivshar, "Fano resonances in all-dielectric oligomers," Nano Lett. **12**, 6459–6463 (2012).
9. Z. Liu, Y. Xu, Y. Lin, J. Xiang, T. Feng, Q. Cao, J. Li, S. Lan, and J. Liu, "High-Q quasibound states in the continuum for nonlinear metasurfaces," Phys. Rev. Lett. **123**, 253901 (2019).
10. A. V. Panov, "Optical Kerr nonlinearity of dielectric nanohole array metasurface in proximity to anapole state," Opt. Lett. **47**, 2866–2869 (2022).
11. A. A. Basharin, M. Kafesaki, E. N. Economou, C. M. Soukoulis, V. A. Fedotov, V. Savinov, and N. I. Zheludev, "Dielectric metamaterials with toroidal response," Phys. Rev. X **5**, 011036 (2014).
12. D. G. Baranov, R. Verre, and P. Karpinski, "Anapole-enhanced intrinsic Raman scattering from silicon nanodisks," ACS Photonics **5**, 2730–2736 (2018).
13. G. B. Lemos, V. Borish, G. D. Cole, S. Ramelow, R. Lapkiewicz, and A. Zeilinger, "Quantum imaging with undetected photons," Nature **512**, 409–412 (2014).
14. E. A. Santos, T. Pertsch, F. Setzpfandt, and S. Saravi, "Subdiffraction quantum imaging with undetected photons," Phys. Rev. Lett. **128**, 173601 (2022).

15. W. Liu, Y. Shi, Z. Yi, C. Liu, F. Wang, X. Li, J. Lv, L. Yang, and P. K. Chu, "Surface plasmon resonance chemical sensor composed of a microstructured optical fiber for the detection of an ultra-wide refractive index range and gas-liquid pollutants," Opt. Express **29**, 40734–40747 (2021).
16. W. Liu, C. Liu, J. X. Wang, J. Lv, Y. Lv, L. Yang, N. An, Z. Yi, Q. Liu, C. Hu, and P. K. Chu, "Surface plasmon resonance sensor composed of microstructured optical fibers for monitoring of external and internal environments in biological and environmental sensing," Results Phys. **47**, 106365 (2023).
17. W. Liu, C. J. Hu, L. Zhou, Z. Yi, C. Liu, J. Lv, L. Yang, and P. K. Chu, "A square-lattice D-shaped photonic crystal fiber sensor based on SPR to detect analytes with large refractive indexes," Phys. E **138**, 115106 (2022).
18. Z. Li, Q. You, J. Li, C. Zhu, L. Zhang, L. Yang, Y. Fang, and P. Wang, "Boosting light-matter interaction in a longitudinal bonding dipole plasmon hybrid anapole system," J. Phys. Chem. C **127**, 3594–3601 (2023).
19. J. Hu, W. Bai, C. Tan, Y. Li, Q. Lin, and L. Wang, "Highly electric field enhancement induced by anapole modes coupling in the dielectric-metal nanoantenna," Opt. Commun. **511**, 127987 (2022).
20. J. Yao, B. Li, G. Cai, and Q. H. Liu, "Doubly mirror-induced electric and magnetic anapole modes in metal-dielectric-metal nanoresonators," Opt. Lett. **46**, 576–579 (2021).
21. J. Lv, H. Zhang, C. Liu, Z. Yi, F. Wang, H. Mu, X. Li, T. Sun, and P. K. Chu, "Optical anapole modes in gallium phosphide nanodisk with forked slits for electric field enhancement," Nanomaterials **11**, 1490 (2021).
22. S. Bhaskar, "Biosensing technologies: a focus review on recent advancements in surface plasmon coupled emission," Micromachines (Basel) **14**, 574 (2023).
23. A. Rai, S. Bhaskar, K. M. Ganesh, and S. S. Ramamurthy, "Hottest hotspots from the coldest cold: welcome to nano 4.0," ACS Appl. Nano Mater. **5**, 12245–12264 (2022).
24. S. Bhaskar, D. Thacharakkal, S. S. Ramamurthy, and C. Subramaniam, "Metal-dielectric interfacial engineering with mesoporous nano-carbon florets for 1000-fold fluorescence enhancements: smartphone-enabled visual detection of perindopril erbumine at a single-molecular level," ACS Sustain. Chem. Eng. **11**, 78–91 (2023).
25. S. Bhaskar, V. Srinivasan, and S. S. Ramamurthy, "Nd_2O_3-Ag nanostructures for plasmonic biosensing, antimicrobial, and anticancer applications," ACS Appl. Nano Mater. **6**, 1129–1145 (2023).
26. S. Bhaskar and S. S. Ramamurthy, "Synergistic coupling of titanium carbonitride nanocubes and graphene oxide for 800-fold fluorescence enhancements on smartphone based surface plasmon-coupled emission platform," Mater. Lett. **298**, 130008 (2021).
27. B. Liu, M. L. Hu, Y. W. Zhang, Y. You, Z. G. Liang, X. N. Peng, and Z. J. Yang, "Strong near-field couplings of anapole modes and the formation of higher-order electromagnetic modes in stacked all-dielectric nanodisks," Chin. Phys. B **31**, 057802 (2022).
28. A. K. Ospanova, A. Karabchevsky, and A. A. Basharin, "Metamaterial engineered transparency due to the nullifying of multipole moments," Opt. Lett. **43**, 503–506 (2018).
29. A. E. Miroshnichenko, A. B. Evlyukhin, Y. F. Yu, R. M. Bakker, A. Chipouline, A. I. Kuznetsov, B. Luk'yanchuk, B. N. Chichkov, and Y. S. Kivshar, "Nonradiating anapole modes in dielectric nanoparticles," Nat. Commun. **6**, 8069 (2015).
30. L. Wei, Z. Xi, N. Bhattacharya, and U. H. Paul, "Excitation of the radiationless anapole mode," Optica **3**, 799–802 (2016).
31. H. W. Mu, Y. Wang, J. Lv, Z. Yi, L. Yang, P. K. Chu, and C. Liu, "Electric field enhancement by a hybrid dielectric-metal nanoantenna with a toroidal dipole contribution," Appl. Opt. **61**, 7125–7131 (2022).
32. X. Zhang, Q. Zhang, Y. Yuan, J. Liu, and X. Liu, "Ultra-directional forward scattering by a high refractive index dielectric T-shaped nanoantenna in the visible," Phys. Lett. A **384**, 126696 (2020).
33. E. D. Palik, *Handbook of Optical Constants of Solids* (Academic, 1985).
34. A. Tripathi, H. R. Kim, P. Tonkaev, S. J. Lee, S. V. Makarov, S. S. Kruk, M. V. Rybin, H. G. Park, and Y. Kivshar, "Lasing action from anapole metasurfaces," Nano Lett. **21**, 6563–6568 (2021).
35. M. Erhard, A. R. Junghans, C. Nair, R. Schwengner, R. Beyer, J. Klug, K. Kosev, A. Wagner, and E. Grosse, "Experimental study of the electric dipole strength in the even Mo nuclei and its deformation depende," Phys. Rev. C **81**, 034319 (2010).
36. Y. Li, Z. Huang, Z. Sui, H. Chen, X. Zhang, H. Guan, W. Qiu, J. Dong, W. Zhu, J. Yu, H. Lu, and Z. Chen, "Optical anapole mode in nanostructured lithium niobate for enhancing second harmonic generation," Nanophotonics **9**, 3575–3585 (2020).
37. K. As'Ham, I. Al-Ani, L. Huang, A. E. Miroshnichenko, and H. T. Hattori, "Boosting strong coupling in a hybrid WSe_2 monolayer–anapole–plasmon system," ACS Photonics **8**, 489–496 (2021).
38. F. Vennberg, A. P. Ravishankar, and S. Anand, "Manipulating light scattering and optical confinement in vertically stacked Mie resonators," Nanophotonics **11**, 4755–4764 (2022).
39. D. Rocco, A. G. Lamprianidis, A. E. Miroshnichenko, and C. D. Angelis, "Giant electric and magnetic Purcell factor in dielectric oligomers," J. Opt. Soc. Am. B **37**, 2738–2744 (2020).
40. J. W. Lv, D. B. Wang, C. Liu, Q. Liu, J. X. Wang, L. Yang, H. W. Mu, and P. K. Chu, "Multiple Fano resonance properties of nanoring-heptamer metal-dielectric structures," Chin. Opt. **16**, 214–227 (2023).
41. K. A. Ospanova, V. M. Cojocari, and A. A. Basharin, "Modified multipoles in photonics," Phys. Rev. B **107**, 035156 (2023).
42. S. Bidault, M. Mivelle, and N. Bonod, "Dielectric nanoantennas to manipulate solid-state light emission," J. Appl. Phys. **126**, 094104 (2019).
43. S. Lepeshov, A. Krasnok, and A. Alu, "Enhanced excitation and emission from 2D transition metal dichalcogenides with all-dielectric nanoantennasm," Nanotechnology **30**, 254004 (2019).
44. Q. Deng, J. Chen, L. Long, B. Chen, H. Yu, and Z. Li, "Silicon cuboid nanoantenna with simultaneous large Purcell factor for electric dipole, magnetic dipole and electric quadrupole emission," Opto-Electron Adv. **5**, 210024 (2022).
45. P. A. Dmitriev, E. Lassalle, L. Ding, Z. Pan, D. C. J. Neo, V. Valuckas, R. Paniagua-Dominguez, J. K. W. Yang, H. V. Demir, and A. I. Kuznetsov, "Hybrid dielectric-plasmonic nanoantenna with multiresonances for subwavelength photon sources," ACS Photonics **10**, 582–594 (2023).
46. Y. Xiong, S. Shepherd, J. Tibbs, A. Bacon, W. Liu, L. D. Akin, T. Ayupova, S. Bhaskar, and B. T. Cunningham, "Photonic crystal enhanced fluorescence: a review on design strategies and applications," Micromachines **14**, 668 (2023).